Superlattices and Microstructures 79 (2015) 116–122

Contents lists available at ScienceDirect

Superlattices and Microstructures

journal homepage: www.elsevier.com/locate/superlattices

# N-structure based on InAs/AlSb/GaSb superlattice photodetectors

M. Hostut [a,*], M. Alyoruk [b], T. Tansel [c], A. Kilic [d], R. Turan [e], A. Aydinli [f], Y. Ergun [d]

[a] Department of Secondary Education of Science & Mathematics, Akdeniz University, Antalya, Turkey
[b] Department of Computer Education and Instructional Technology, Dumlupınar University, Kutahya, Turkey
[c] Institute of Nuclear Sciences, Hacettepe University, Ankara, Turkey
[d] Department of Physics, Anadolu University, Eskisehir, Turkey
[e] Department of Physics, Middle East Technical University, Ankara, Turkey
[f] Department of Physics, Bilkent University, Ankara, Turkey

ARTICLE INFO

*Article history:*
Received 29 October 2014
Received in revised form 19 December 2014
Accepted 22 December 2014
Available online 30 December 2014

*Keywords:*
Infrared detector
III–V semiconductors
Type-II superlattice
InAs/AlSb/GaSb
Photodetectors
MWIR

ABSTRACT

We have studied the theoretical and experimental properties of InAs/AlSb/GaSb based type-II superlattice (T2SL) pin photodetector called N-structure. Electronic properties of the superlattice such as HH–LH splitting energies was investigated using first principles calculations taking into account InSb and AlAs as possible interface transition alloys between AlSb/InAs layers and individual layer thicknesses of GaSb and InAs. T2SL N-structure was optimized to operate as a MWIR detector based on these theoretical approaches tailoring the band gap and HH–LH splitting energies with InSb transition layers between InAs/AlSb interfaces. Experimental results show that AlSb layers in the structure act as carrier blocking barriers reducing the dark current. Dark current density and $R_0A$ product at 125 K were obtained as $1.8 \times 10^{-6}$ A cm$^{-2}$ and 800 Ω cm$^2$ at zero bias, respectively. The specific detectivity was measured as $3 \times 10^{12}$ Jones with cut-off wavelengths of 4.3 μm at 79 K reaching to $2 \times 10^9$ Jones and 4.5 μm at 255 K.



* Corresponding author. Tel.: +90 242 3106075; fax: +90 242 2261953.
*E-mail address:* mhostut@akdeniz.edu.tr (M. Hostut).

http://dx.doi.org/10.1016/j.spmi.2014.12.022
0749-6036/

## 1. Introduction

6.1 Å family of semiconductors (InAs/GaSb/AlSb) is highly desirable for realization of high performance T2LS photodetectors operating at high temperatures (HOT) to be used in infrared applications since it offers flexible combination of constituent alloys. Band alignment of the T2SL system leads to the spatial localization of electrons in InAs and holes in GaSb layers. On the other hand, large gap material AlSb may be used as a carrier barrier whose conduction band offset is higher than that of GaSb and valence band offset is slightly higher than that of InAs. By varying the thickness of constituent materials, the band gap of superlattice can be tailored over a wide spectral range between 2 and 30 μm which covers short-to-very long infrared wavelengths in the atmospheric window [1,2]. There have been numbers of high performance photodetector architectures reported in the literature. These include p-i-n structures [3–5] and heterojunctions such as nBn [6,7], pBp [8], CBIRD [9], M-structure [10] and review of barrier detectors [11].

Proper combination of constituent alloys in the T2SL system and band gap engineering may enable the design of high performance detectors with unipolar electron barriers and the requirement of third generation imaging systems operating at higher temperatures. For this purpose we designed new T2SL photodetector with unipolar electron barrier called N-structure. N-structure is a InAs/AlSb/GaSb based T2SL p-i-n photodetector [12] where two mono layers (MLs) of thin AlSb layers are placed in between InAs and GaSb layers in contrast with M structure [13] having AlSb barriers placed in the GaSb layers of the InAs/GaSb T2SL system. Layer sequences in growth direction and the schematic band diagram of N-structure are shown in Fig. 1(a) and (b) respectively. AlSb layer in the structure acting as a barrier plays important role. First, AlSb barrier pushes carriers towards GaSb/InAs interface to increase electron and hole wavefunction overlap, enhancing type-II optical transition under reverse bias (Fig. 2). Second, acting as an electron blocking barrier, AlSb blocks the thermally generated carriers to reduce the diffusion current. Third, G-R current may also be suppressed down to cryogenic temperatures since AlSb is a large band gap material with a large electron effective mass. Therefore, optical and electrical performances are improved by N-structure design. In this report, we present the theoretical and experimental results for the new design N-structure photodetector. Electronic properties of N-structure such as HH–LH splitting energies are investigated by taking into account the constituent layer thicknesses and possible interface transition layers such as InSb and AlAs between InAs/AlSb interfaces. Experimental results on electrical and optical performance of the N-structure photodetector

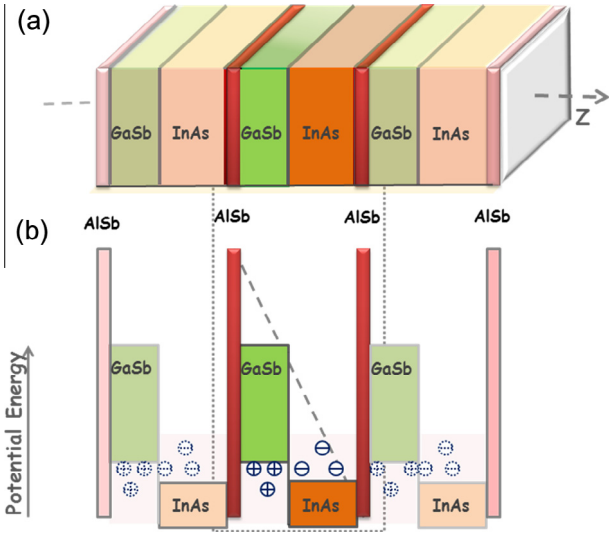


**Fig. 1.** (a) Layer sequence in growth direction, (b) conduction and valence band profiles for N-structure.

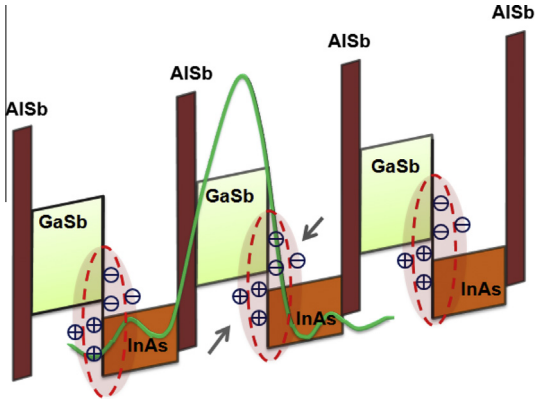


**Fig. 2.** Conduction and valence band profiles for N-structure with electron and hole confinement under reverse bias. Overlap integral (green line) is given in the center of the structure. (For interpretation of the references to color in this figure legend, the reader is referred to the web version of this article.)

are discussed under higher operating temperatures. The paper is organized as follows. We outline the theory and calculations of first principle approximations in Section 2. Experimental details are given in Section 3. Finally, experimental results and the major conclusions are drawn for this study in Sections 4 and 5.

## 2. Theory and calculations

Calculations have been performed with the ABINIT code which is based on the density functional theory [14]. The results were obtained under the local density approximation (LDA) where, for the exchange–correlation interactions, we use the Perdew–Wang parameterization [15], which reproduces the quantum Monte Carlo electron gas data of Ceperley and Alder [16]. For the pseudopotential, the valence configurations of the constituent atoms were chosen as In ($5s^2$ $5p^1$), As ($4p^3$ $4s^2$), Al ($3s^2$ $3p^1$), Sb ($5s^2$ $5p^3$), and Ga ($4s^2$ $4p^1$). In order to get accurate results for the investigated properties of the structure the plane wave cutoff energy of 50 Ha and $8 \times 8 \times 4$ $k$-point grid were used in the calculations.

Due to ~1.3% lattice mismatch and having no common atom at the InAs and AlSb interface, growth of AlSb layers on InAs layers are highly stressed in InAs/AlSb/GaSb T2SL structure. If the critical thickness is exceeded (>10 nm), this may led defects [17], so we only placed two MLs of AlSb between InAs and GaSb layers in our calculations. As far as interface transition materials concern between InAs and AlSb layers, there are two possible interface transition materials that are a ML of In–Sb and Al–As. DFT results show that InAsAl ($c/a$ = 1.00117) (0.117% or 1170 ppm) has less tensile strain than InSbAl ($c/a$ = 1.003217) (~0.322% or 3220 ppm) both in growth and in-plane directions. These values are not higher than that of a standard T2SL structure with InAs/GaSb interface (0.62%) [18]. HRXRD results show that the mismatch between SL and GaSb substrate was 1566 ppm (~0.16%). This can be attributed to not having common atom between AlSb and InAs layers in InAs/AlSb/GaSb T2SL structure [12].

We also study the effect of AlSb blocking barrier on heavy hole-light hole (HH–LH) splitting energies of the InAs/AlSb/GaSb based T2SL N-structure by using first principles approach. The influence of both InSb and AlAs interface structures on HH–LH splitting energies is analyzed by band structure calculations of the $(InAs)_n/(AlSb)_2/(GaSb)_{n-2}$ ($n$ = 3–8) superlattices. The energy separation of the HH–LH splitting energy is particularly important in the suppression of nonradiative electron–hole recombination in practical detector applications. Electronic structure calculations indicate that HH–LH splitting energies of these systems with AlAs interfaces are greater than that of the structures with InSb interfaces (see in Table 1).

**Table 1**
HH–LH splitting energies of $(InAs)_n/(AlSb)_2/(GaSb)_{n-2}$ structure for AlAs and InSb interfaces.

| Number of MLs ($n$) | HH–LH (meV) (AlAs Interface) | HH–LH (meV) (InSb Interface) |
|---|---|---|
| 3 | 186 | 44 |
| 4 | 193 | 72 |
| 5 | 187 | 90 |
| 6 | 180 | 97 |
| 7 | 169 | 101 |
| 8 | 157 | 97 |

Calculated LH, HH and conduction band effective mass ($m_{lh}$, $m_{hh}$, $m_c$) values of $(InAs)_n/(AlSb)_2/(GaSb)_{n-2}$ superlattices are given in Fig. 3. The figure also includes bulk alloys of AlSb, InAs and GaSb, both with their calculated and experimental effective mass values at the $\Gamma$ point as inset for comparison. Calculated and experimental values for the bulk alloys show similar behaviors. They are close to each other except for AlSb which shows indirect band gap, and does not have conduction band minima at the $\Gamma$ point. If the effective mass values of bulk and superlattice structures are compared, it can be easily seen that the superlattice $m_{hh}$ values show exponential decrease according to bulk ones while $m_{lh}$ and $m_c$ of superlattice have bigger values then their bulk equivalents. For the superlattice structures the effective masses are not dependent on the interface type. The difference between the $m_{hh}$ effective mass values of InSb and AlAs interfaced structures are getting smaller with the increasing number of layers. Also, the $m_c$ values are directly proportional to the layer thickness of the $(InAs)_n/(AlSb)_2/(GaSb)_{n-2}$ superlattice structures. These results show similar behaviors with the M-structure calculations investigated by Razeghi et al. [19] for fixed AlSb layer thickness.

## 3. Experimental details

The superlattice photodiode was grown by commercially (IQE Inc. USA) with molecular beam epitaxy. First a 100 nm GaSb buffer layer is deposited on unintentionally p-type doped (100) GaSb substrate followed by a 20 nm lattice matched $Al_{0,4}Ga_{0,6}As_{0,04}Sb_{0,96}$ buffer layer. 1000 nm thick p-type GaSb:Be ($p = 1 \times 10^{17}$ cm$^{-3}$) bottom contact is grown on the buffer layer. The p–i–n detector structure consists of 9/2/8.5 MLs) of InAs/AlSb/GaSb SL layers as 90 periods of p-region with GaSb:Be ($p = 1.5 \times 10^{17}$ cm$^{-3}$), 60 period of i-intrinsic region and 40 periods of n-region with InAs:Te ($n = 5 \times 10^{17}$ cm$^{-3}$). The device is terminated by 20 nm InAs: Te n-contact ($n = 5 \times 10^{17}$ cm$^{-3}$).

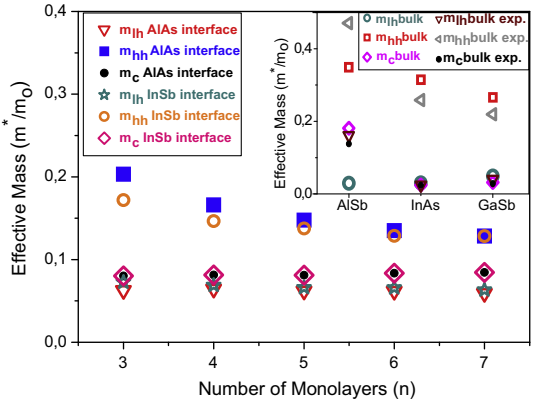


**Fig. 3.** Calculated light hole ($m_{lh}$), heavy hole ($m_{hh}$) and conduction ($m_c$) band effective mass values of $(InAs)_n/(AlSb)_2/(GaSb)_{n-2}$ superlattice. Inset shows the effective masses for bulk structures with their experimental values at $\Gamma$ point. Experimental values are taken from Ref. [22].

Standard lithography was used to define square mesas with different dimensions. Phosphoric acid based solution was used for the etch process in order to minimize the surface leakage current. The wafer was etched through the T2SL structure and stopped in the bottom contact. The fabrication details can be given elsewhere [20]. Plasma enhanced chemical vapor deposition (PECVD) system has been used to deposit a 250 nm thick protective $SiO_2$ layer at 160 °C with 2% $SiH_4/N_2$ and $N_2O$ gas flows of 180 sccm and 225 sccm, respectively. 5 nm Titanium (Ti) and 200 nm Gold (Au) were deposited for both top and bottom Ohmic contacts. Devices were then wire bonded a leadless chip carrier for further characterization. Electrical performance of the N-structure design superlattice barrier structure have been investigated by using a HP4142OA source-measure unit. Samples were mounted on a He cooled closed cycle cold finger with a cold shield system. Dark current measurements were performed at various temperatures. The responsivity of the detector has been measured using calibrated blackbody source (Newport, Oriel 67,000), lock-in amplifier (SRS, SR830 DSP) and mechanical chopper (SRS, SR540) system.

## 4. Results and discussion

Temperature dependent electrical and optical characterizations were performed on 500 × 500 $\mu m^2$ mesa-based pin diodes. Fig. 4 (a) and (b) show the current–voltage and corresponding dynamic resistance area product ($R_dA$)-voltage characteristics of the sample at high operating temperature regime from 125 to 271 K. At 125 K and under zero bias, dark current density and $R_0A$ are $1.8 \times 10^{-6}$ A $cm^{-2}$ and 800 Ω $cm^2$, whereas at 271 K, dark current density and $R_0A$ are $1.23 \times 10^{-5}$ A $cm^{-2}$ and 140 Ω $cm^2$, respectively. These results are very promising for high temperature FPA operations. At an operating bias voltage of −0.3 V and 77 K temperature, dark current density and $R_dA$ are measured as $5.3 \times 10^{-7}$ A $cm^{-2}$ and $3.7 \times 10^5$ Ω $cm^2$. These high electrical performance values of the detector structure offer excellent operating conditions at cryogenic temperatures. These performance characteristics prove that InAs/AlSb interfaces in the detector structure indicates good crystalline property. Fig. 4 (c) shows the inverse temperature (1000/T) dependence of $R_dA$ product under −50 mV bias. In the temperature range 271–100 K, the $R_dA$ reveals diffusion-limited behavior (Arrhenius type) with associated activation energy of 270 meV which is close to the band gap energy. In the lower temperature range (100–50 K), the dominant mechanism starts to become generation recombination (GR) which mostly depends on the density of deep level traps inside the bandgap (Eg/2). For temperature lower than 50 K, defect-related mechanism probably dominates the $R_dA$ curve. The responsivity spectra of single pixel detector were measured under an operating bias of −0.3 V using a calibrated blackbody source at 450 K. Fig. 5 shows the responsivity spectra at various temperatures. The observed peak responsivities (and 50% cut-off wavelengths ($\lambda_c$)) for temperatures 79, 125 and 255 K are 0.35 (4.2), 0.375 (4.3), and 0.2 A $W^{-1}$ (4.5 μm), respectively. The detectivity ($D^*$) of the device was calculated by using following equation:

$$D^* = R_p(A\Delta f)^{-0.5}/i_n \tag{1}$$

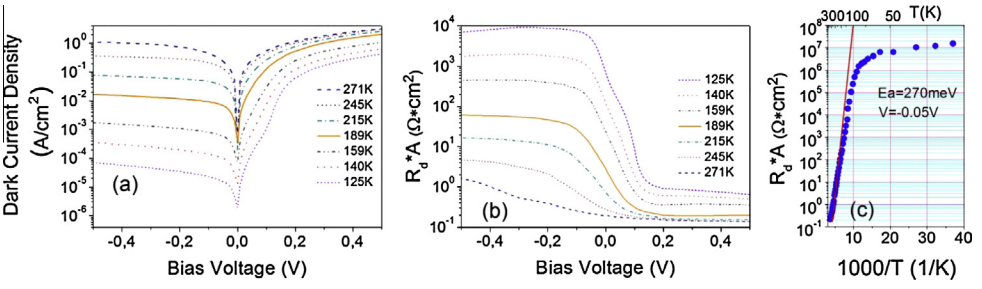


**Fig. 4.** Bias voltage dependence of (a) dark current densities, (b) $R_dA$ at various temperatures, and (c) inverse temperature (1000/T) vs $R_dA$ for N-structure.

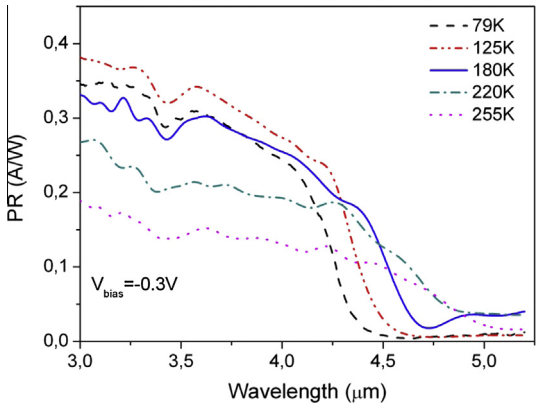


**Fig. 5.** Responsivity spectra for N-structure at various temperatures.

where $R_p$ is the peak responsivity, $i_n$ is the dark noise current ($i_n = (2qI\Delta f + 4kT\Delta f/R_d)^{0.5}$), $k$ is the Boltzmann's constant, $I$ is the dark current, $R_d$ is dynamic resistance, $\Delta f$ is the bandwidth over which the noise is measured, and $A$ is the optical area of the device. In the case of zero bias operating mode, $D^*$ was calculated by using the Johnson noise formula i.e., $i_n = (4kT\Delta f/R_0)^{0.5}$. Fig. 6 shows the temperature dependence $D^*$ measured at 4 μm as well as background limited performance (BLIP) $D^*$ value for an operating bias of −0.3 V. The detector shows BLIP at temperature below 125 K with the BLIP $D^*$ of $2.6 \times 10^{10}$ Jones under 300 K background. At 77 K, the device achieves a $D^*$ of $3 \times 10^{12}$ Jones which is two orders of magnitude higher than that of BLIP $D^*$. We estimate that the detector shows $D^*$ of $3 \times 10^{10}$ Jones above the BLIP $D^*$ of $2.6 \times 10^{10}$ Jones at 180 K. At 255 K, the $D^*$ is measured as $2 \times 10^9$ Jones which is similar to the performance of other MWIR type-II superlattices nBn detectors grown on GaSb [21]. These are very promising values for the detector under high temperature operations. Inset also shows spectral $D^*$ of the device taken at 79 K and zero bias conditions. The spectral $D^*$ at 4 μm is measured as high as $6.2 \times 10^{13}$ Jones reaching to the peak value of $1 \times 10^{14}$ Jones at 3 μm.

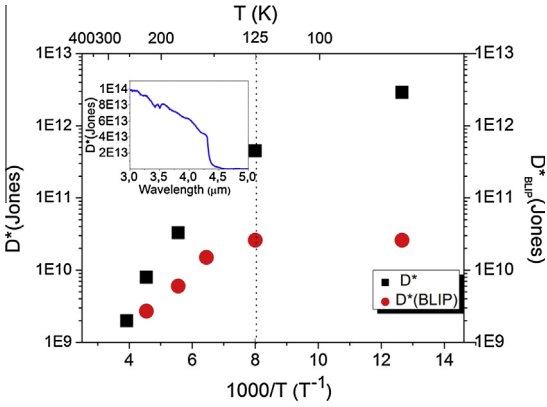


**Fig. 6.** Temperature dependence of $D^*$ and BLIP $D^*$. The dashed line represents the BLIP temperature. Inset shows the spectral $D^*$ measured under zero bias and 79 K.

## 5. Conclusion

We report on theoretical and experimental studies of InAs/AlSb/GaSb based T2SL N-structure. The electronic properties of N-structure such as HH–LH splitting energies are investigated by first principles approximations as a function of constituent layer thicknesses of GaSb and InAs with possible interface transition materials of InSb and AlAs at InAs/AlSb interfaces. Experimental results show that the AlSb barrier in the structure provides excellent optical and electrical performance values. Under BLIP conditions, the device structure shows dark current density, $R_dA$ and $D^*$ such as $4.8 \times 10^{-5}$ A cm$^{-2}$, $1 \times 10^4\,\Omega\,\mathrm{cm}^2$ and $4.65 \times 10^{11}$ Jones under operating bias of $-0.3$ V at 125 K, respectively. The results are encouraging us to investigate for the long wavelength detectors in the future.

## Acknowledgements

Y. Ergun acknowledges the supports of TUBITAK and Anadolu University (Grants from Tubitak: 109T072 and BAP: 1104F073-1104F074-1404F249). M. Hostut and A. Kilic also acknowledge the supports of Akdeniz University (BAP Grant: 2012.01.0110.002) and Anadolu University (BAP Grant: 1305F108) respectively.

## References

[1] A.M. Hoang, G. Chen, A. Haddadi, S.A. Pour, M. Razeghi, Appl. Phys. Lett. 100 (2012) 211101.
[2] H.J. Haugan, G.J. Brown, S. Elhamri, W.C. Mitchel, K. Mahalingam, M. Kim, G.T. Noe, N.E. Ogden, J. Kono, Appl. Phys. Lett. 101 (2012) 171105.
[3] R. Rehm, M. Walther, J. Schmitz, F. Rutz, J. Fleißner, R. Scheibner, J. Ziegler, Infrared Phys. Technol. 52 (2009) 344–347.
[4] J.B. Rodriguez, C. Cervera, P. Christol, Appl. Phys. Lett. 97 (2010) 251113.
[5] F. Rutz, R. Rehm, M. Walther, J. Schmitz, L. Kirste, A. Wörl, J.M. Masur, R. Scheibner, J. Ziegler, Infrared Phys. Technol. 54 (2011) 237–242.
[6] J.B. Rodriguez, E. Plis, G. Bishop, Y.D. Sharma, H. Kim, L.R. Dawson, S. Krishna, Appl. Phys. Lett. 91 (2007) 043514.
[7] E. Plis, B.J. Rodriguez, G.D. Bishop, Y.D. Sharma, A. Kroshakhlagh, L.R. Dawson, J. Bundas, R. Cook, D. Burrows, R. Dennis, K. Patnaude, A. Reisinger, M. Sundaram, S. Krishna, Proc. SPIE 6940 (2008) 69400E.
[8] E. Plis, S. Krishna, N. Gautam, S. Myers, IEEE Photonic J. 3 (2011) 234–240.
[9] D.Y. Ting, C.J. Hill, A. Soibel, S.A. Keo, J.M. Mumolo, J. Nguyen, S.D. Gunapala, Appl. Phys. Lett. 95 (2009) 023508.
[10] M. Razeghi, S.A. Pour, E. Huang, G. Chen, A. Haddadi, B.M. Nguyen, Proc. SPIE 8012 (2011) 80122Q.
[11] P. Martyniuk, M. Kopytko, A. Rogalski, Opto-Electron. Rev. 22 (2014) 127.
[12] O. Salihoglu, A. Muti, K. Kutluer, T. Tansel, R. Turan, Y. Ergun, A. Aydinli, Appl. Phys. Lett. 101 (2012) 073505.
[13] M. Razeghi, B.M. Nguyen, WIO '07: 6th International Workshop on Information Optics (Reykjavik, Iceland) 35 (2007).
[14] X. Gonze, B. Amadon, et al, Comput. Phys. Commun. 180 (2009) 2582–2615.
[15] J.P. Perdew, Y. Wang, Phys. Rev. B 45 (1992) 13244–13249.
[16] D.M. Ceperley, Phys. Rev. Lett. 45 (1980) 566–569.
[17] J. Spitzer, H.D. Fuchs, P. Etchegoin, M. Ilg, M. Cardona, B. Brar, H. Kroemer, Appl. Phys. Lett. 62 (1993) 2274–2276.
[18] B.Z. Nosho, B.R. Bennett, L.J. Whitman, M. Goldenberg, J. Vac. Sci. Tech. B 19 (2001) 1626–1630.
[19] B.M. Nguyen, M. Razeghi, V. Nathan, G.J. Brown, Proc. SPIE 6479 (2007) 64790S.
[20] O. Salihoglu, A. Muti, K. Kutluer, T. Tansel, R. Turan, A. Aydinli, J. Appl. Phys. 111 (2012) 074509.
[21] H.S. Kim et al, Appl. Phys. Lett. 92 (2008) 183502.
[22] S. Adachi, Properties of Semiconductor Alloys: Group-IV, III–V and II–VI Semiconductors, 1st edn., Willey & Suns Ltd., UK, 2009.